Theoretical Analysis of the Doppler System Test

J. R. Lesh
Network Operations Office

In this article, models for the doppler extraction and measurement processes used in the doppler system test are formulated and analyzed. The purpose of the article is to acquaint operations personnel with the doppler system, as well as the corresponding system test criteria.

I. Introduction

To verify operational readiness of a system, one usually performs a series of tests. However, the results of these tests are of little value unless they can be correlated with theoretically predicted values based on an analytical model of the system. In this discussion, models for the doppler extraction and measurement processes are formulated and analyzed to enable comparisons between the experimental and theoretical results of the doppler system test (Ref. 1).

We begin in Section II by creating a mathematical model for the doppler extractor portion of the receiver/exciter subsystem. In Section III, a model for the doppler counter/resolver assembly (along with the phase residual computation) is formulated. Both of these models are then used in Section IV to obtain a theoretical jitter expression for each of the three basic test configurations.

In Section V, the expressions of Section IV are evaluated using typical test configuration parameters. A set of theoretical jitter curves is provided for direct comparison with experimentally determined values. Finally, in Section VI, some additional sources of measurement error are discussed.

Throughout this article, it is assumed that all phase error functions (after phase drift terms have been extracted) are independent processes having zero mean values and can be described completely by second-order statistics.

II. Doppler Extraction Model

The extraction of doppler signals is performed in the receiver/exciter subsystem. The receiver portion of this subsystem provides this extraction with the aid of reference signals supplied from the exciter and the frequency and timing subsystem (FTS). Fig. 1 shows a block diagram of the portions of the exciter and FTS which provide these reference signals to the receiver. In this figure, as in subsequent figures, we will use circled numbers or subscribed Ss placed in triangles to denote specific signals. The difference between these notations is that the circled numbers are used to identify signals at a specific point

within a figure, while the triangle notation is used to identify signals which pass between two or more figures.

Let us define the reference standard output (Fig. 1) as[1]

$$① = \cos(\omega_{RS}t + \theta_{RS}(t)) \tag{1}$$

where ω_{RS} is the natural reference standard frequency in radians/sec (typically 5.0 MHz $= \pi \times 10^7$ rad/sec) and $\theta_{RS}(t)$ is the reference standard phase (jitter) function in radians. In this case, the 1-MHz and 1-pulse/sec (PPS) outputs can be represented by

$$S_1 = \cos\left(2\pi \times 10^6 t + \frac{2\pi}{\omega_{RS}} \times 10^6 \theta_{RS}(t)\right) \tag{2}$$

and

$$S_2 = \cos\left(2\pi t + \frac{2\pi}{\omega_{RS}} \theta_{RS}(t)\right) \tag{3}$$

The reference signal ① is also used to drive the exciter voltage-controlled oscillator (VCO), which will produce an output of the form

$$② = \cos(\omega_e t + \theta_e(t))$$

where ω_e is the natural VCO output frequency and $\theta_e(t)$ is the VCO (jitter) function. Consequently, the remaining receiver reference signals are

$$S_3 = \cos\left(\frac{57}{221}\omega_e t + \frac{57}{221}\theta_e(t)\right) \tag{4}$$

and

$$S_4 = \cos(3\omega_e t + 3\theta_e(t)) \tag{5}$$

Now consider the block diagram of the receiver shown in Fig. 2. The receiver input signal is assumed to be of the form

$$S_5 = \cos(\omega_R t + \omega_D t + \psi(t)) \tag{6}$$

where ω_R is the no-doppler downlink angular frequency, ω_D is the angular doppler frequency shift, and $\psi(t)$ is the receiver input phase function. Let us also define the output of the local oscillator as

$$③ = \cos(\omega_{LO}t + \theta_{LO}(t)) \tag{7}$$

If we now define the phase error at the output of the loop phase detector by

$$④ = \phi(t) \tag{8}$$

then it is clear that the first mixer output at point ⑤ is given by

$$⑤ = \sin\left[\frac{5}{2}(\omega_{LO}t + \theta_{LO}(t)) - \phi(t) + \pi\right] \tag{9}$$

Since the input to the first mixer is also specified, we also have the signal at point ⑥ as

$$⑥ = \cos\left[\frac{1}{32}\left(\omega_R + \omega_D - \frac{5}{2}\omega_{LO}\right)t + \frac{1}{32}\left(\phi(t) + \psi(t) - \frac{5}{2}\theta_{LO}(t) - \frac{\pi}{2}\right)\right] \tag{10}$$

The third multiple of the loop VCO is now passed to the doppler extractor subassembly, where it is first mixed with the signals S_4 and S_3. From Eqs. (4) and (5), we have

$$⑦ = \cos\left\{\left[\frac{1}{32}\left(\omega_R + \omega_D - \frac{5}{2}\omega_{LO}\right) - 3\omega_e\right]t + \left[\frac{1}{32}\left(\phi(t) + \psi(t) - \frac{5}{2}\theta_{LO}(t) - \frac{\pi}{2}\right) - 3\theta_e(t)\right]\right\} \tag{11}$$

and

$$⑧ = \cos\left\{\left[\left(\frac{8\cdot 57}{221} + 24\right)\omega_e - \frac{1}{4}\omega_R - \frac{1}{4}\omega_D + \frac{5}{8}\omega_{LO}\right]t + \left[\left(\frac{8\cdot 57}{221} + 24\right)\theta_e(t) - \frac{1}{4}\psi(t) - \frac{1}{4}\phi(t) + \frac{5}{8}\theta_{LO}(t) + \frac{\pi}{8}\right]\right\} \tag{12}$$

Now, if we return to the expression for the local oscillator output, it is clear that the signals at ⑨ and ⑩ are given by

$$⑨ = \cos\left(\frac{5}{8}\omega_{LO}t + \frac{5}{8}\theta_{LO}(t)\right) \tag{13}$$

and

$$⑩ = \cos\left(\frac{5}{2}\omega_{LO}t + \frac{5}{2}\theta_{LO}(t)\right) \tag{14}$$

[1]In this model, we will find that the sinusoidal parameters of interest are the frequency and phase. Since the amplitudes are unimportant, we will assume all amplitudes have been normalized to 1.

After mixing the signal ⑩ with the 1-MHz bias signal from S_1, we obtain signal ⑪

$$⑪ = \cos\left(\frac{5}{2}\omega_{LO}t + 2\pi \times 10^6 t + \frac{5}{2}\theta_{LO}(t) + \frac{2\pi}{\omega_{RS}} \times 10^6 \theta_{RS}(t)\right) \quad (15)$$

With the above signals specified, we can now determine expressions for the doppler quantities produced by the receiver. The first of these is the biased doppler output S_6 produced by the mixing signal ⑪ with the fourth multiple of ⑧ in the biased doppler detector. The detected signal, which consists primarily of the doppler shift frequency plus the 1-MHz bias signal, is given by

$$S_6 = \cos\left\{\left[2\pi \times 10^6 + \omega_R - \left(\frac{32 \cdot 57}{221} + 32 \cdot 3\right)\omega_e + \omega_D\right]t + \left[\phi(t) + \psi(t) - \left(\frac{32 \cdot 57}{221} + 32 \cdot 3\right)\theta_e(t) + \frac{2\pi \times 10^6}{\omega_{RS}}\theta_{RS}(t) - \frac{\pi}{2}\right]\right\} \quad (16)$$

The other doppler quantities are produced by the dual-phase detector and are sometimes called the UHF doppler outputs. These outputs S_7 and S_8 are orthogonal outputs consisting primarily of one-fourth the doppler shift frequency and are given by

$$S_7 = \cos\left\{\left[\frac{\omega_D}{4} + \frac{\omega_R}{4} - \left(\frac{8 \cdot 57}{221} + 24\right)\omega_e\right]t + \left[\frac{\phi(t)}{4} + \frac{\psi(t)}{4} - \left(\frac{8 \cdot 57}{221} + 24\right)\theta_e(t) - \frac{\pi}{8}\right]\right\} \quad (17)$$

and

$$S_8 = \cos\left\{\left[\frac{\omega_D}{4} + \frac{\omega_R}{4} - \left(\frac{8 \cdot 57}{221} + 24\right)\omega_e\right]t + \left[\frac{\phi(t)}{4} + \frac{\psi(t)}{4} - \left(\frac{8 \cdot 57}{221} + 24\right)\theta_e(t) + \frac{3\pi}{8} + \theta_{DD}\right]\right\} \quad (18)$$

where θ_{DD} is a constant and is the quadrature mismatch of the 0- and 90-degree detector outputs.

Before proceeding, it is necessary to make a comment about the receiver phase error $\phi(t)$. In the derivation, we have not as yet given an expression for $\phi(t)$. This is to allow $\phi(t)$ not only to represent the receiver phase error due to noise, but also to include internal VCO loop noise $\phi_i(t)$, that is,

$$\phi(t) = \phi_n(t) + \phi_i(t) \quad (19)$$

III. Doppler Counter/Resolver Model

The doppler counter/resolver assembly operates in conjunction with the receiver to perform a period counting of the biased doppler signal. A simplified block diagram of the counter/resolver is shown in Fig. 3. A timing diagram of the assembly is shown in Fig. 4, which will be helpful in creating a mathematical model.

The counter/resolver receives the biased doppler signal S_6 from the receiver, shapes this signal to a digital pulse stream, and applies the resulting signal to the doppler counter. This counter is a non-destructive counter which will increment by one every time a positive-going transition of the biased doppler signal is encountered. In addition to this counter, there is a resolver counter, which is a destructive counter driven from a high-frequency oscillator. The resolver is used to provide additional phase information for the doppler counting operation. The enabling of the resolver counter and the transferring of the two counter values to the digital instrumentation subsystem (DIS) computer are controlled by the sampling signal S_2 (usually the 1-PPS signal), as well as the positive transitions of the biased doppler signal.

To determine the characteristics of the counter/resolver assembly, refer to Fig. 4. At time $t_{D_{k-1}}$, a transfer count pulse is generated which transfers the values of the doppler counter and the resolver counter to the DIS computer and then resets the resolver counter. From this point on until the next sample pulse (usually the 1-PPS signal), the resolver counter is disabled. The doppler counter, however, counts continuously during all intervals. At the next sample pulse, occurring at time t_k, the resolver is reenabled and will count the number of cycles of an internal oscillator of frequency f_{DR} (usually 100 MHz) until the next positive transition of the biased doppler signal is encountered. At this time, t_{D_k}, a new transfer count pulse is generated which transfers the values of the doppler and resolver counters to the DIS and resets the resolver counter, and the process is then repeated. To determine statistics for the counter/resolver outputs at S_9 and S_{10} would be an extremely difficult task. However, if we include in our model the portion of the DIS software which uses S_9 and S_{10} to compute phase residuals, the task will be greatly simplified.

With this description of the counting operations at hand, let us consider the biased doppler signal as given by

$$\text{(S}_6\text{)} = \cos\left[Wt + \Phi(t)\right] \tag{20}$$

where

$$W = 2\pi \times 10^6 + \omega_R - \left(\frac{32 \cdot 57}{221} + 3 \cdot 32\right)\omega_e + \omega_D \tag{21}$$

and

$$\Phi(t) = \phi(t) + \psi(t) - \left(\frac{32 \cdot 57}{221} + 3 \cdot 32\right)\theta_e(t) + \frac{2\pi \times 10^6}{\omega_{RS}}\theta_{RS}(t) - \frac{\pi}{2} \tag{22}$$

Now, from Fig. 4, we note that, in the interval between any two transfer count pulses, the doppler counter counts an integral number of biased doppler cycles. Thus, if we let C_k represent the doppler counter value at time t_{D_k}, then the doppler counter residual at time t_{D_k}, $(\widetilde{C}_k - \widetilde{C}_{k-1})$ expressed in radians, is given by

$$\begin{aligned}(\widetilde{C}_k - \widetilde{C}_{k-1}) &= 2\pi(C_k - C_{k-1}) \\ &= W(t_{D_k} - t_{D_{k-1}}) + \Phi(t_{D_k}) - \Phi(t_{D_{k-1}})\end{aligned} \tag{23}$$

Now consider the operation of the resolver. Since the enabling and disabling of the resolver are not necessarily coherent with the internal resolver oscillator operating at f_{DR} (Hz), the value in the resolver N_{R_k} at time t_{D_k} will be

$$N_{R_k} = f_R(t_{D_k} - t_k) \pm 1 \qquad \text{(counts or cycles)} \tag{24}$$

where the ± 1 denotes the maximum error resulting from the non-coherent time quantization. The resolver count can then be related to an equivalent phase angle C_{R_k} of the biased doppler signal by

$$\begin{aligned}C_{R_k} &= \frac{N_{R_k}}{f_{DR}}\left[W + \frac{\Phi(t_{D_k}) - \Phi(t_k)}{t_{D_k} - t_k}\right] \qquad \text{(radians)} \\ &= W(t_{D_k} - t_k) + \Phi(t_{D_k}) - \Phi(t_k) + \varepsilon_k\end{aligned} \tag{25}$$

where ε_k is the equivalent quantization error, which has a maximum value of

$$|\varepsilon_k|_{\max} = \frac{1}{f_{DR}}\left[W + \frac{\Phi(t_{D_k}) - \Phi(t_k)}{t_{D_k} - t_k}\right] \tag{26}$$

Finally, the residual at time t_{D_k}, denoted R_k, is given by

$$R_k = (\widetilde{C}_k - \widetilde{C}_{k-1}) - (C_{R_k} - C_{R_{k-1}}) \tag{27}$$

which, after substituting Eqs. (23) and (25), becomes

$$R_k = W(t_k - t_{k-1}) + \Phi(t_k) - \Phi(t_{k-1}) - \varepsilon_k + \varepsilon_{k-1} \tag{28}$$

It is interesting to note that, if one neglects the ε terms, Eq. (28) produces exactly the phase change of the biased doppler signal in the sampling interval t_{k-1} to t_k.

IV. Specified Test Configurations

A. Fully Coherent Configuration

In the fully coherent configuration (test translator modes), the exciter VCO signal at point (2) is used to generate the S-band signal. From Fig. 5, we see directly that the S-band signal which is the receiver input signal is given by

$$\begin{aligned}\text{(S}_{11}\text{)} &= \text{(S}_5\text{)} \\ &= \cos\left[\left(\frac{32 \cdot 57}{221} + 96\right)\omega_e + \left(\frac{32 \cdot 57}{221} + 96\right)\theta_e(t)\right]\end{aligned} \tag{29}$$

Comparing this with Eq. (6) implies

$$\left.\begin{aligned}\omega_R &= \left(\frac{32 \cdot 57}{221} + 96\right)\omega_e \\ \omega_D &= 0 \\ \psi(t) &= \left(\frac{32 \cdot 57}{221} + 96\right)\theta_e(t)\end{aligned}\right\} \tag{30}$$

Using these results, we have the biased doppler signal given by

$$\text{(S}_6\text{)} = \cos\left\{2\pi \times 10^6 t + \phi(t) + \frac{2\pi \times 10^6}{\omega_{RS}}\theta_{RS}(t) - \frac{\pi}{2}\right\} \tag{31}$$

Finally, the residual process R_k is given by Eq. (28) with the parameters

$$W = 2\pi \times 10^6 \tag{32}$$

$$\Phi(t) = \phi(t) + \frac{2\pi \times 10^6}{\omega_{RS}}\theta_{RS}(t) - \frac{\pi}{2}$$

Thus, we have

$$\begin{aligned}R_k &= 2\pi \times 10^6(t_k - t_{k-1}) + \phi(t_k) - \phi(t_{k-1}) \\ &\quad + \frac{2\pi \times 10^6}{\omega_{RS}}\left[\theta_{RS}(t_k) - \theta_{RS}(t_{k-1})\right] - \varepsilon_k + \varepsilon_{k-1}\end{aligned} \tag{33}$$

Furthermore, if we assume that

$$\theta_{RS}(t) = (\Delta\omega)\,t + \theta'_{RS}(t) \tag{34}$$

where $\theta'_{RS}(t)$ contains no constant frequency offset (i.e., zero mean) and if $\omega_{RS} = \pi \times 10^7$, then

$$R_k = \left(2\pi \times 10^6 + \frac{\Delta\omega}{5}\right)(t_k - t_{k-1}) + \phi(t_k) - \phi(t_{k-1}) + \frac{\theta'_{RS}(t_k) - \theta'_{RS}(t_{k-1})}{5} - \varepsilon_k + \varepsilon_{k-1} \tag{35}$$

Now, since

$$E\{R_k\} = \left(2\pi \times 10^6 + \frac{\Delta\omega}{5}\right)(t_k - t_{k-1}) \tag{36}$$

the variance of R_k (assuming $\phi(t_k)$, $\phi(t_{k-1})$, $\theta'_{RS}(t_k)$, $\theta'_{RS}(t_{k-1})$, ε_k, and ε_{k-1} are all independent) is

$$\mathrm{Var}\{R_k\} = 2\sigma_\phi^2 + \frac{2}{25}\sigma^2_{\dot{\theta}_{RS}} + 2\sigma_\varepsilon^2 \tag{37}$$

where σ_ϕ^2 is the variance of the receiver phase error, $\sigma^2_{\dot{\theta}_{RS}}$ is the variance of the reference standard zero-mean phase error, and σ_ε^2 is the variance of the doppler resolver quantization error given by

$$\sigma_\varepsilon^2 = \frac{1}{12}\left\{\frac{1}{f_{DR}}\left[2\pi \times 10^6 + \frac{\Delta\omega}{5} + \frac{\Phi(t_{D_k}) - \Phi(t_k)}{t_{D_k} - t_k}\right]\right\}^2 \approx \frac{\pi^2 \times 10^{12}}{3f_{DR}^2} \tag{38}$$

Finally, we note that the doppler test software removes the effects of double sampling and then computes the rms jitter of the residuals in degrees. The corresponding theoretical value is given by

$$\text{Theoretical jitter, degrees rms} = \frac{360}{2\pi}\sqrt{\sigma_\phi^2 + \frac{1}{25}\sigma^2_{\dot{\theta}_{RS}} + \sigma_\varepsilon^2} \tag{39}$$

B. Semi-Coherent Configuration

In the semi-coherent (test transmitter coherent) configuration (see Fig. 6), an additional synthesizer is used to produce the S-band signal. However, both the spare synthesizer and the exciter are driven by the same reference standard. If we let the synthesizer output at point (12) be given by

$$(12) = \cos(\omega_{SY}t + \theta_{SY}(t)) \tag{40}$$

then we can express this signal in terms of the reference signal (1) by

$$(12) = \cos\left[\frac{\omega_{SY}}{\omega_{RS}}(\omega_{RS}t + \theta_{RS}(t))\right] \tag{41}$$

The S-band signal is then given by

$$S_{12} = S_5 = \cos\left[120\omega_{SY}t + \frac{120\omega_{SY}}{\omega_{RS}}\theta_{RS}(t)\right] \tag{42}$$

Comparing this with Eq. (6) indicates that

$$\left.\begin{aligned}\omega_R + \omega_D &= 120\omega_{SY}\\ \psi(t) &= \frac{120\omega_{SY}}{\omega_{RS}}\theta_{RS}(t)\end{aligned}\right\} \tag{43}$$

Consequently, the biased doppler signal is given by

$$S_6 = \cos\left\{\left[2\pi \times 10^6 + 120\omega_{SY} - \left(\frac{57 \cdot 32}{221} + 3 \cdot 32\right)\omega_e\right]t + \phi(t) + \frac{120\omega_{SY}}{\omega_{RS}}\theta_{RS}(t) - \left(\frac{57 \cdot 32}{221} + 3 \cdot 32\right)\theta_e(t) + \frac{2\pi \times 10^6}{\omega_{RS}}\theta_{RS}(t) - \frac{\pi}{2}\right\} \tag{44}$$

Thus, the residual process is given by

$$R_k = \left[2\pi \times 10^6 + 120\omega_{SY} - \left(\frac{32 \cdot 57}{221} + 3 \cdot 32\right)\omega_e\right] \times (t_k - t_{k-1}) + \phi(t_k) - \phi(t_{k-1}) + \frac{120\omega_{SY}}{\omega_{RS}}[\theta_{RS}(t_k) - \theta_{RS}(t_{k-1})] - \left(\frac{32 \cdot 57}{221} + 3 \cdot 32\right)[\theta_e(t_k) - \theta_e(t_{k-1})] + \frac{2\pi \times 10^6}{\omega_{RS}}[\theta_{RS}(t_k) - \theta_{RS}(t_{k-1})] - \varepsilon_k + \varepsilon_{k-1} \tag{45}$$

Again we let

$$\theta_{RS}(t) = (\Delta\omega)\,t + \theta'_{RS}(t)$$

and

$$\omega_{RS} = \pi \times 10^7$$

Furthermore, we let

$$\theta_e(t) = \frac{\omega_e}{\omega_{RS}}(\Delta\omega)\,t + \theta'_e(t) \tag{46}$$

where $\theta'_e(t)$ is a zero-mean phase process. Thus, the residual is given by

$$R_k = \left[2\pi \times 10^6 + 120\omega_{SY}\left(1 + \frac{\Delta\omega}{10\pi \times 10^6}\right) - \left(\frac{32 \cdot 57}{221} + 3 \cdot 32\right)\omega_e\left(1 + \frac{\Delta\omega}{10\pi \times 10^6}\right) + \frac{\Delta\omega}{5}\right] \times (t_k - t_{k-1}) + \phi(t_k) - \phi(t_{k-1}) + \frac{120\omega_{SY}}{\omega_{RS}}[\theta'_{RS}(t_k) - \theta'_{RS}(t_{k-1})] - \left(\frac{32 \cdot 57}{221} + 3 \cdot 32\right)[\theta'_e(t_k) - \theta'_e(t_{k-1})] + \frac{1}{5}[\theta'_{RS}(t_k) - \theta'_{RS}(t_{k-1})] - \varepsilon_k + \varepsilon_{k-1} \quad (47)$$

Hence, the mean and variance of R_k are given by

$$E(R_k) = \left[2\pi \times 10^6 + 120\omega_{SY}\left(1 + \frac{\Delta\omega}{10\pi \times 10^6}\right) - \left(\frac{32 \cdot 57}{221} + 3 \cdot 32\right)\omega_e\left(1 + \frac{\Delta\omega}{10\pi \times 10^6}\right) + \frac{\Delta\omega}{5}\right] \quad (48)$$

and

$$\mathrm{Var}\{R_k\} = 2\sigma_\phi^2 + 2\left(\frac{120\omega_{SY}}{10\pi \times 10^6} + \frac{1}{5}\right)^2 \sigma^2_{\theta'_{RS}} + 2\left(\frac{57 \cdot 32}{221} + 3 \cdot 32\right)^2 \sigma^2_{\theta'_e} + 2\sigma_\varepsilon^2 \quad (49)$$

Therefore, the theoretical jitter is

$$\text{Theoretical jitter, degrees rms} = \frac{360}{2\pi}\sqrt{\sigma_\phi^2 + \left(\frac{120\omega_{SY}}{10\pi \times 10^6} + \frac{1}{5}\right)^2 \sigma^2_{\theta'_{RS}} + \left(\frac{57 \cdot 32}{221} + 3 \cdot 32\right)^2 \sigma^2_{\theta'_e} + \sigma_\varepsilon^2} \quad (50)$$

C. Incoherent Configuration

In the incoherent (test transmitter incoherent) configuration (see Fig. 7), the system model is the same as that in the semi-coherent configuration, except the synthesizer is now driven by a separate reference standard. If we denote the output of the second reference standard at (1′) by

$$(1') = \cos[\omega_{SS}t + \theta_{SS}(t)] \quad (51)$$

then the spare synthesizer output is given by

$$(12) = \cos\left[\omega_{SY}t + \frac{\omega_{SY}}{\omega_{SS}}\theta_{SS}(t)\right] \quad (52)$$

In this case, the receiver input becomes

$$S_5 = \cos\left[120\omega_{SY}t + 120\frac{\omega_{SY}}{\omega_{SS}}\theta_{SS}(t)\right] \quad (53)$$

and, hence, the biased doppler signal is

$$S_6 = \cos\left\{\left[2\pi \times 10^6 + 120\omega_{SY} - \left(\frac{57 \cdot 32}{221} + 3 \cdot 32\right)\omega_e\right]t + \phi(t) + 120\frac{\omega_{SY}}{\omega_{SS}}\theta_{SS}(t) - \left(\frac{57 \cdot 32}{221} + 3 \cdot 32\right)\theta_e(t) + \frac{2\pi \times 10^6}{\omega_{RS}}\theta_{RS}(t) - \frac{\pi}{2}\right\} \quad (54)$$

Computing the residual with $\omega_{RS} = \omega_{SS} = \pi \times 10^7$ gives

$$R_k = \left[2\pi \times 10^6 + 120\omega_{SY} - \left(\frac{57 \cdot 32}{221} + 3 \cdot 32\right)\omega_e\right] \times (t_k - t_{k-1}) + \phi(t_k) - \phi(t_{k-1}) + \frac{120\omega_{SY}}{10\pi \times 10^6}[\theta_{SS}(t_k) - \theta_{SS}(t_{k-1})] - \left(\frac{57 \cdot 32}{221} + 3 \cdot 32\right)[\theta_e(t_k) - \theta_e(t_{k-1})] + \frac{1}{5}\theta_{RS}(t_k) - \frac{1}{5}\theta_{RS}(t_{k-1}) - \varepsilon_k + \varepsilon_{k-1} \quad (55)$$

Again we will extract the frequency uncertainty from the reference standard phase functions. However, since there are two standards, we will subscribe the $\Delta\omega$ terms according to

$$\theta_{RS}(t) = (\Delta\omega_{RS})t + \theta'_{RS}(t)$$
$$\theta_{SS}(t) = (\Delta\omega_{SS})t + \theta'_{SS}(t) \quad (56)$$

The residual process then becomes

$$R_\kappa = \left\{2\pi \times 10^6 + 120\omega_{SY}\left(1 + \frac{\Delta\omega_{SS}}{10\pi \times 10^6}\right) - \left(\frac{57 \cdot 32}{221} + 3 \cdot 32\right)\omega_e\left(1 + \frac{\Delta\omega_{RS}}{10\pi \times 10^6}\right) + \frac{\Delta\omega_{RS}}{5}\right\} \times (t_k - t_{k-1}) + \phi(t_k) - \phi(t_{k-1}) + \frac{120\omega_{SY}}{10\pi \times 10^6}[\theta'_{SS}(t_k) - \theta'_{SS}(t_{k-1})] - \left(\frac{57 \cdot 32}{221} + 3 \cdot 32\right)[\theta'_e(t_k) - \theta'_e(t_{k-1})] + \frac{\theta'_{RS}(t_k)}{5} - \frac{\theta'_{RS}(t_{k-1})}{5} - \varepsilon_k + \varepsilon_{k-1} \quad (57)$$

with a mean value

$$E\{R_k\} = \left\{2\pi \times 10^6 + 120\omega_{SY}\left(1 + \frac{\Delta\omega_{SS}}{10\pi \times 10^6}\right) - \left(\frac{57 \cdot 32}{221} + 3 \cdot 32\right)\omega_e\left(1 + \frac{\Delta\omega_{RS}}{10\pi \times 10^6}\right) + \frac{\Delta\omega_{RS}}{5}\right\}(t_k - t_{k-1}) \quad (58)$$

and variance

$$\mathrm{Var}\{R_k\} = 2\sigma_\phi^2 + 2\left(\frac{120\omega_{SY}}{10\pi \times 10^6}\right)^2 \sigma^2_{\theta'_{SS}} + 2\left(\frac{57 \cdot 32}{221} + 3 \cdot 32\right)^2 \sigma^2_{\theta'_e} + \frac{2}{25}\sigma^2_{\theta'_{RS}} + 2\sigma_\varepsilon^2 \quad (59)$$

and the theoretical jitter becomes

$$\text{Theoretical jitter, degrees rms} = \frac{360}{2\pi}\sqrt{\sigma_\phi^2 + \left(\frac{120\omega_{SY}}{10\pi \times 10^6}\right)^2 \sigma^2_{\theta'_{SS}} + \left(\frac{57 \cdot 32}{221} + 3 \cdot 32\right)^2 \sigma^2_{\theta'_e} + \frac{\sigma^2_{\theta'_{RS}}}{25} + \sigma_\varepsilon^2} \quad (60)$$

V. Calculation of Theoretical Jitter

In Section IV, an expression for the rms phase jitter was developed for each of the basic configurations in terms of the quantities σ_ϕ^2, $\sigma^2_{\theta'_{RS}}$, $\sigma^2_{\theta'_e}$, $\sigma^2_{\theta'_{SS}}$, σ_ε^2, and ω_{SY}. In this section, we will examine these quantities in more detail and then evaluate the rms jitter expressions.

As previously mentioned, the receiver phase error contains the effects of both the received thermal noise and the internally generated loop noise. In other words,

$$\sigma_\phi^2 = \sigma_n^2 + \sigma_l^2 \quad (61)$$

where σ_n^2 is the phase error variance due to receiver input noise and σ_l^2 is the phase error variance due to internal contributions. The first of these expressions can be determined (Ref. 2, Chapter 10) by solving the set of equations

$$\sigma_n^2 = \frac{\Gamma}{m\gamma^2}\left[\frac{1 + \left(\frac{\alpha}{\alpha_0}\right)\gamma r_0}{1 + r_0}\right]; \qquad \gamma = \frac{[1 - \exp(-\sigma_n^2)]}{\sigma_n^2} \quad (62)$$

where m is the receiver margin above design-point threshold and

$$\Gamma = \frac{1 + \rho_H}{0.862 + \rho_H} \quad (63)$$

(The remaining terms are defined in Ref. 2.)

The determination of σ_l^2, however, requires a little more effort. Bunce (Ref. 3) has shown that

$$\sigma_l^2 = f\left(\frac{\alpha_0}{\alpha}\right)\sigma^2_{0N_0} \quad (64)$$

where

$$f\left(\frac{\alpha_0}{\alpha}\right) = \begin{cases} \dfrac{\left(\frac{\alpha_0}{\alpha}\right)^2\left[1 - \frac{2}{\pi}\tan^{-1}\left(\dfrac{1 - \frac{\alpha_0}{\alpha}}{\sqrt{\frac{2\alpha_0}{\alpha} - 1}}\right)\right]}{\sqrt{\frac{2\alpha_0}{\alpha} - 1}}; & \dfrac{\alpha}{\alpha_0} < 2 \\ \dfrac{1}{\pi}; & \dfrac{\alpha}{\alpha_0} = 2 \\ \dfrac{\left(\frac{\alpha_0}{\alpha}\right)^2\left[\ln\left(\dfrac{1 - \frac{\alpha_0}{\alpha} + \sqrt{1 - \frac{2\alpha_0}{\alpha}}}{1 - \frac{\alpha_0}{\alpha} - \sqrt{1 - \frac{2\alpha_0}{\alpha}}}\right)\right]}{\pi\sqrt{1 - \frac{2\alpha_0}{\alpha}}}; & \dfrac{\alpha}{\alpha_0} > 2 \end{cases} \quad (65)$$

and $\sigma^2_{\delta N_0}$ is the phase error variance of the receiver when measured at very strong signal levels but in the design point bandwidth. Unfortunately, $\sigma^2_{\delta N_0}$ is not specified in the system performance specifications. Instead, the combined effect of the exciter VCO loop, multipliers, and receiver loop is specified with the receiver operating at a strong signal level and the bandwidth adjusted to its design-point value. However, since the exciter has a bandwidth (10 Hz) which is approximately equal to the receiver design-point bandwidth (12 Hz), we will assume that the receiver contribution and exciter contribution are equal; i.e.,

$$\sigma^2_{\delta N_0} = \left(\frac{57 \cdot 32}{221} + 3 \cdot 32\right)^2 \sigma^2_{\theta' e} \tag{66}$$

Furthermore, we have from Ref. 4 that

$$\sigma^2_{\delta N_0} + \left(\frac{57 \cdot 32}{221} + 3 \cdot 32\right)^2 \sigma^2_{\theta' e} = 0.0195 \quad \text{(radians}^2\text{)} \tag{67}$$

so that

$$\sigma^2_{\delta N_0} = \left(\frac{57 \cdot 32}{221} + 3 \cdot 32\right)^2 \sigma^2_{\theta' e} = 0.00975 \quad \text{(radians}^2\text{)} \tag{68}$$

The remaining parameters can be determined much more easily. For example, we can assume that both reference standards have the same phase statistics; thus, from the reference standard specifications, we have

$$\sigma^2_{\theta' \mathrm{RS}} = \sigma^2_{\theta' \mathrm{SS}} = 2.47 \times 10^{-8} \quad \text{(radians}^2\text{)} \tag{69}$$

Secondly, the spare synthesizer will normally be operated at a frequency of 19 MHz; thus,

$$\omega_{\mathrm{SY}} = 1.194 \times 10^8 \quad \text{(radians/sec)}$$

Finally, we note from Eq. (38) that, if the biased doppler signal is approximately 1.0 MHz and the resolver internal oscillator operates at 100 MHz, the quantization error variance is given by

$$\sigma^2_\varepsilon = \frac{(3.6)^2}{12} \quad \text{(degrees}^2\text{)}$$

$$= 3.29 \times 10^{-4} \quad \text{(radians}^2\text{)} \tag{70}$$

The rms jitter of the test translator modes (Eq. 39) has been computed using the above values and is shown in Fig. 8.[2] In Fig. 9, the rms jitter for the test transmitter modes (Eq. 50 or 60) is shown. We note that Fig. 9 suffices for both Eq. (50) and Eq. (60) since they differ only in the placement of the $\sigma^2_{\theta' \mathrm{RS}}/5$ term, a quantity which, compared to the others, is extremely small.

VI. Measurement Error Sources

Thus far, we have considered only the quantities which an ideal rms jitter estimator would obtain. However, in practice the estimator suffers from a number of "real world" limitations. For example, the rms jitter is estimated by forming a sample variance on the residuals; i.e., the estimated jitter $\hat{\sigma}$ is given by

$$\hat{\sigma} = \frac{360}{2\pi}\left[\frac{1}{2N}\sum_{k=1}^{N}\left(R_k - \frac{1}{N}\sum_{j=1}^{N} R_j\right)^2\right]^{1/2} \tag{71}$$

where N is the number of residuals used in the calculation. By computing the expected value of $\hat{\sigma}$, we get

$$\sqrt{E\{\hat{\sigma}^2\}} = \sigma_{\mathrm{actual}} \cdot \sqrt{1 - \frac{2}{N^2}} \tag{72}$$

which shows that the estimator has a bias factor of $\sqrt{1 - (2/N^2)}$. However, if N is large (say 100), this factor becomes insignificant. Furthermore, the estimator will have some variance around this mean value. The computation of this variance is quite time-consuming due to the fact that adjacent residuals are correlated. However, we can overbound the variance by assuming that every other residual is independent and that the intermediate residuals provide no information. Thus, the estimator itself will have an rms error given by

$$\text{rms error} < \frac{\sqrt{2}\,\sigma_{\mathrm{actual}}}{\sqrt{N}} \tag{73}$$

Finally, we must note that the theoretical values used for comparison with the experimental values will also contain some errors. These errors result from the incompleteness of the models and from the inaccuracies with which one measures system parameters (receiver margin, loop bandwidth, etc.). As an example, the receiver margin is usually not known to within < 0.3 dB. Unfortunately, these effects cannot be easily modeled, and hence one is forced to add "engineering" factors to the theoretical jitter limits.

[2]In practice, one will usually not observe rms jitter values as small as the strong signal result of Fig. 8. The error results from the uniform quantizing error assumption, which breaks down when the receiver rms jitter is less than about 5 degrees. One often observes strong signal jitter values as much as 2 degrees rms above the strong signal value of Fig. 8.

References

1. Barnes, G. D., *Doppler System Evaluation Test*, Document 853-32-2B-11. Jet Propulsion Laboratory, Pasadena, Calif. (in process as JPL internal document).
2. Tausworthe, R. C., *Theory and Practical Design of Phase-Locked Receivers*, Technical Report 32-819, Vol. I. Jet Propulsion Laboratory, Pasadena, Calif., Feb. 15, 1966.
3. Bunce, R., "Effect of VCO Noise on Phase Lock Receiver," in *The Deep Space Network for the Period November 1 to December 31, 1969*, Space Programs Summary 37-61, Vol. II, pp. 115–120. Jet Propulsion Laboratory, Pasadena, Calif., Jan. 31, 1970.
4. *Deep Space Network/Flight Project Interface Design Handbook*, Document 810-5, Rev. C. Jet Propulsion Laboratory, Pasadena, Calif., Apr. 1972 (JPL internal document).

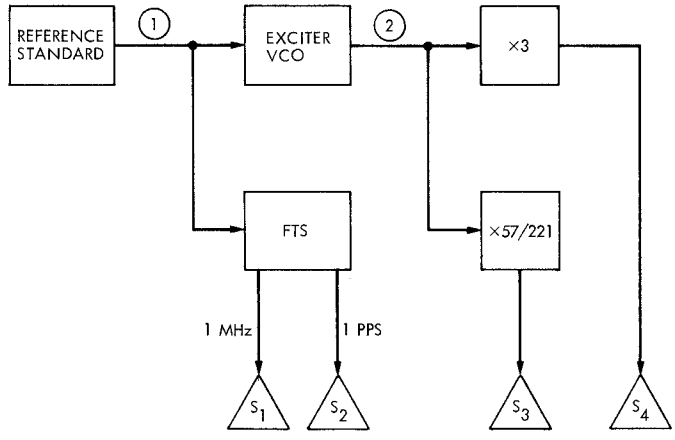

Fig. 1. Block diagram of the generation of receiver reference signals from the exciter and FTS

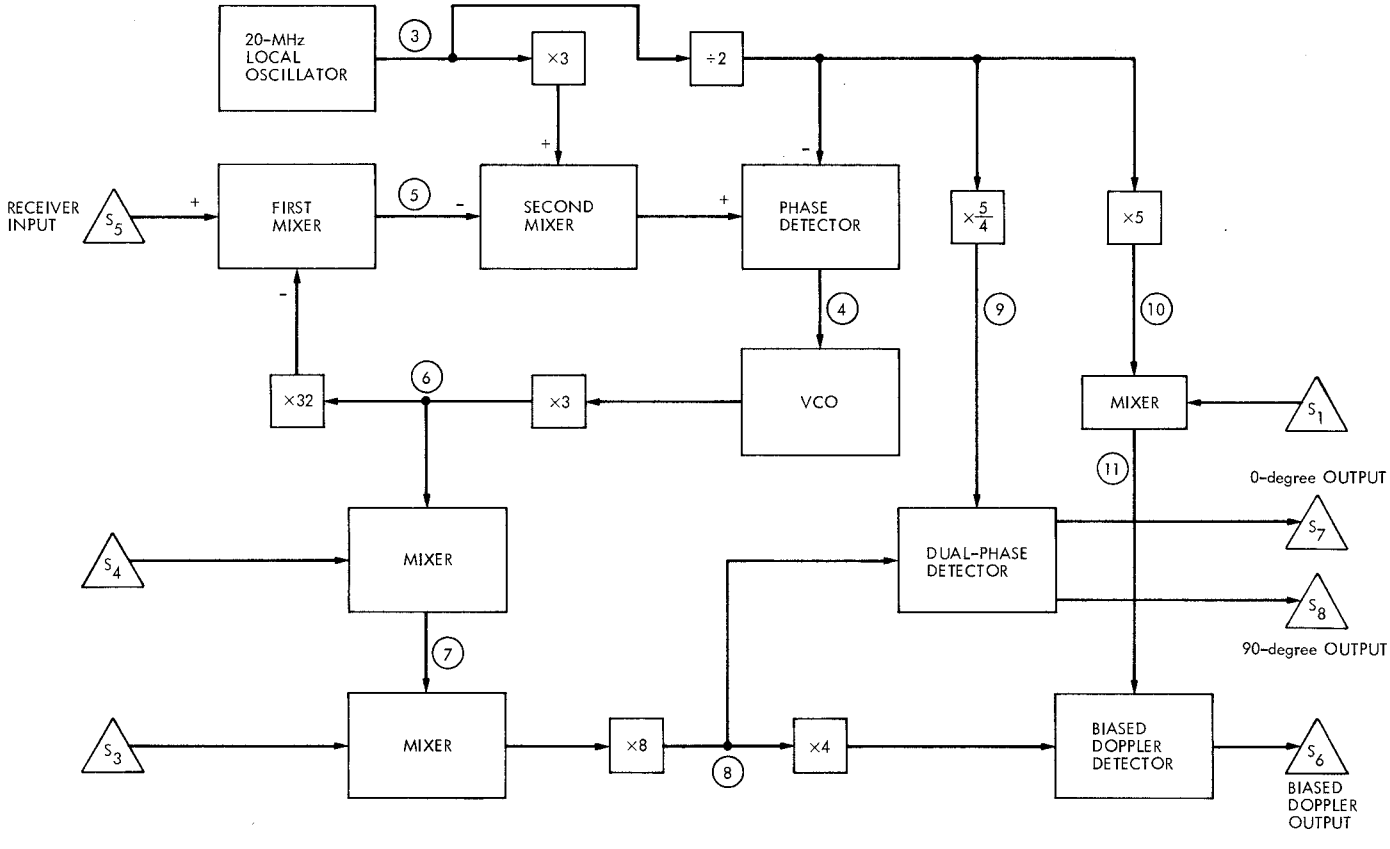

Fig. 2. Block diagram of receiver and doppler extractor

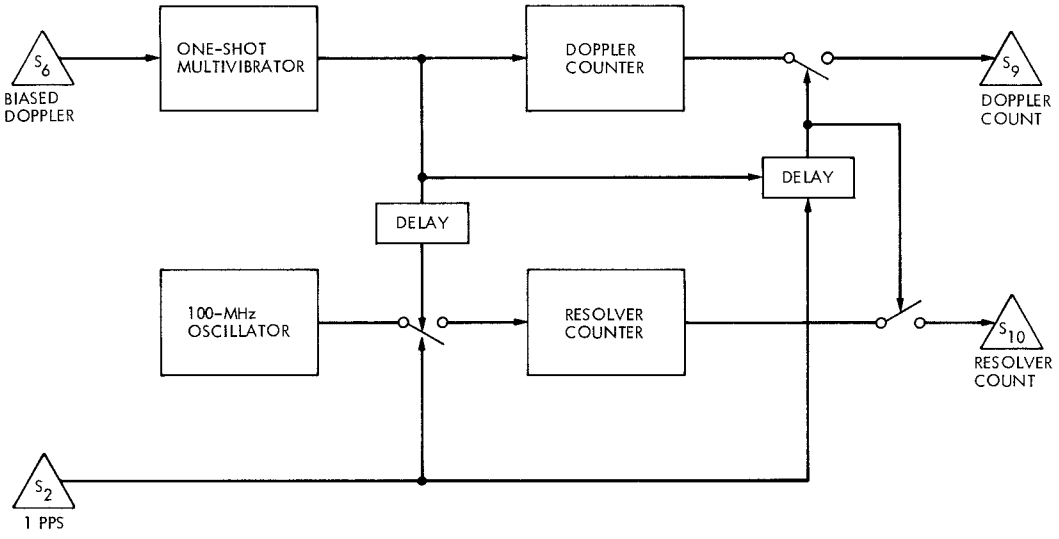

Fig. 3. Block diagram of doppler counter/resolver

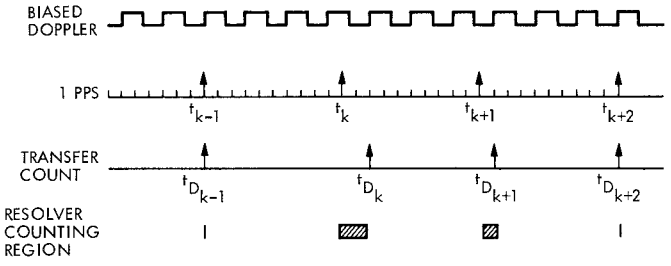

Fig. 4. Timing diagram of doppler counter/resolver

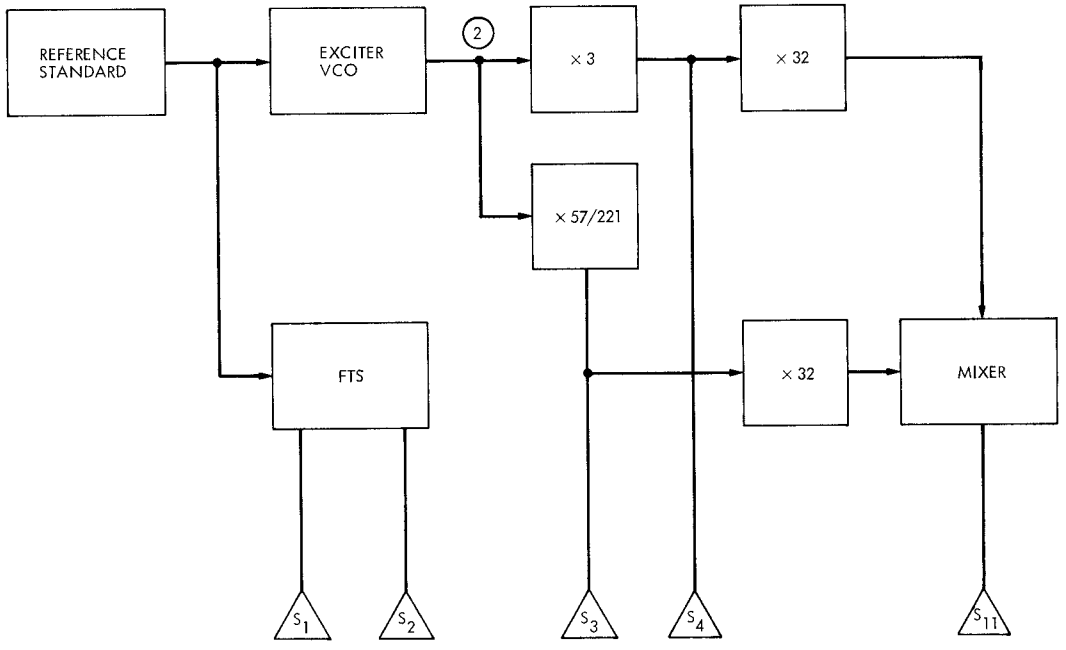

Fig. 5. Block diagram of receiver reference generation for test translator modes

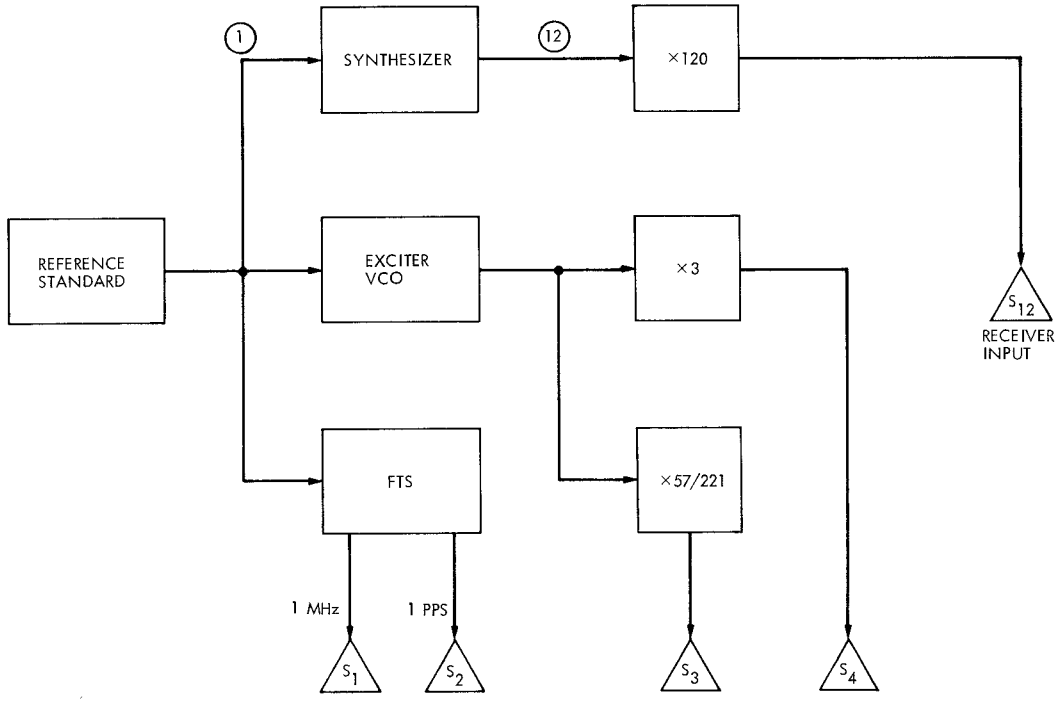

Fig. 6. Block diagram of receiver reference generation for test transmitter coherent mode

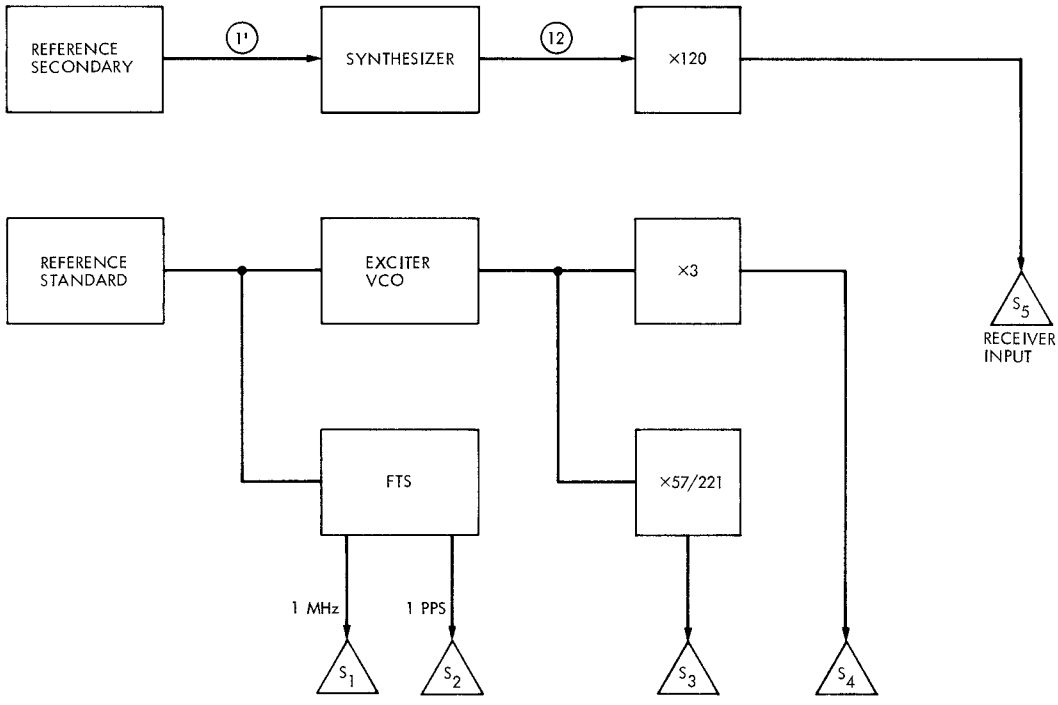

Fig. 7. Block diagram of receiver reference generation for test transmitter incoherent mode

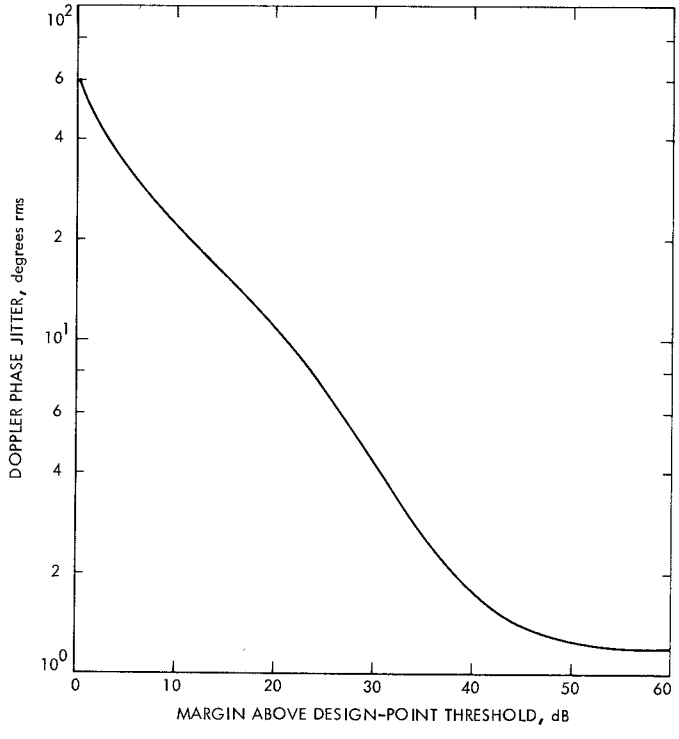

Fig. 8. Theoretical doppler jitter for test translator modes

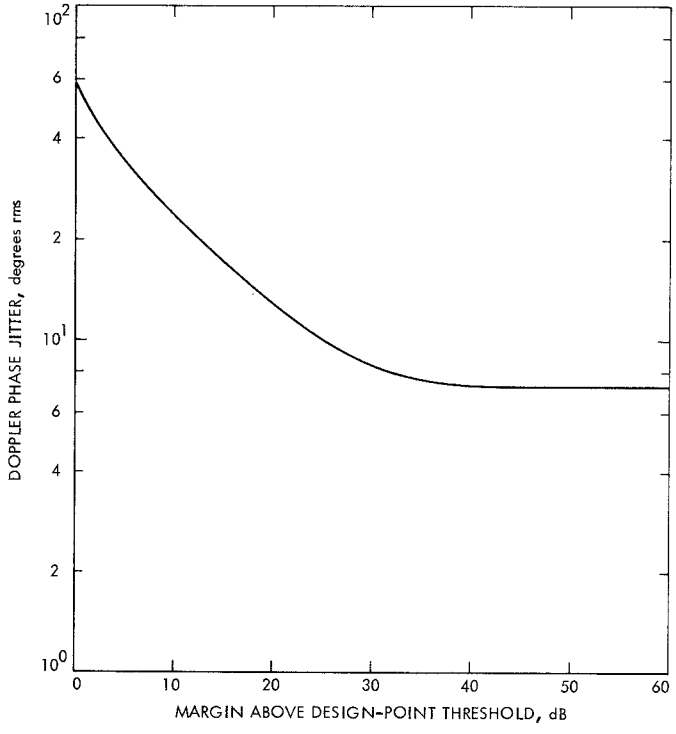

Fig. 9. Theoretical doppler jitter for test transmitter modes